Supporting Information for *Unusual phase behaviour for organo-halide perovskite nanoparticles synthesized by reverse micelle templating*

M. Munir[1], A. Salib[1], L.S. Hui[2], and A. Turak[1,2] *
[1] Department of Physics, Centre for NanoScience Research, Concordia University, Montreal, QC, H4B 1R6, Canada
[2] Department of Engineering Physics, McMaster University, 1280 Main St. W, Hamilton, Canada, L8S 4L7
ayse.turak@concordia.ca, turaka@mcmaster.ca; Tel.: +1-514-848-2424 x3276

The following supplementary details are available free of charge.

- Comparison of AFM images of particle arrays before and after O_2 plasma treatment.
- Comparison of PL for various precursor salt ratios for MAPI
- AFM and spatial statistic images of MAPI nanoparticles from different precursor ratios.
- PL of micelle encapsulated nanoparticle showing stability characteristics
- PL and XRD for PyI-PbBr precursor combinations
- Nanostress developed in the micelle due to MAI infiltration as determined by QNM measurements

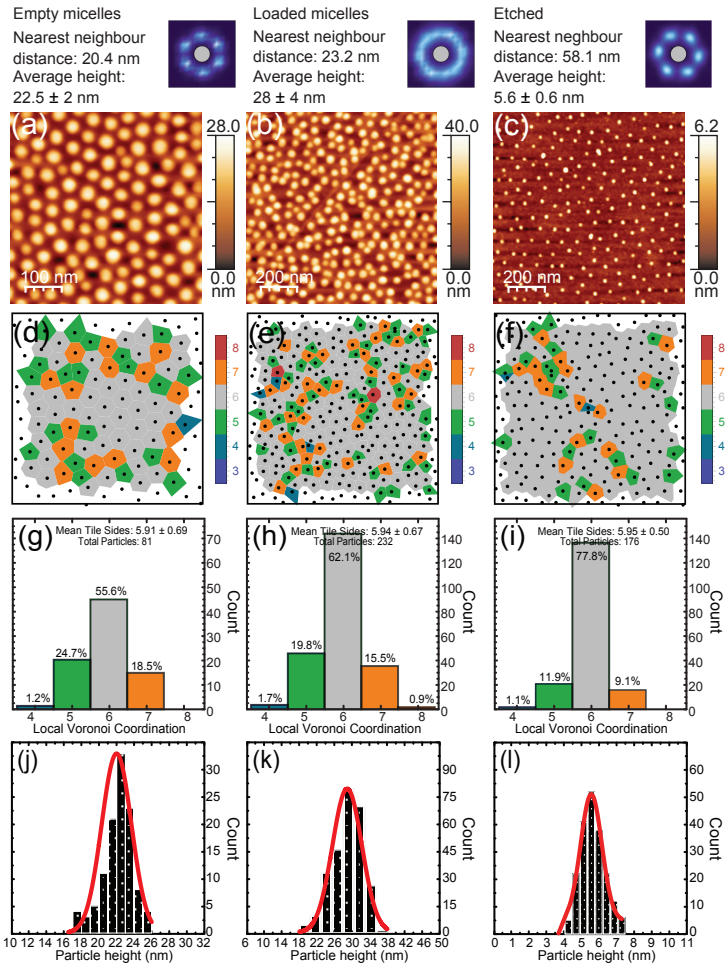

Figure S1 (a-c) AFM images of unloaded, and loaded polymer micelles before and after oxygen plasma treatment for $MAPbBr_3$ nanoparticles. (d-f) The Voronoi tessellations are used to quantify the nanoparticle order where the colour indicates the number of nearest neighbours (g-i) The probability distribution with respect to number of nearest neighbours of the Voronoi tesselation. (j-l) Histogram of particle heights.

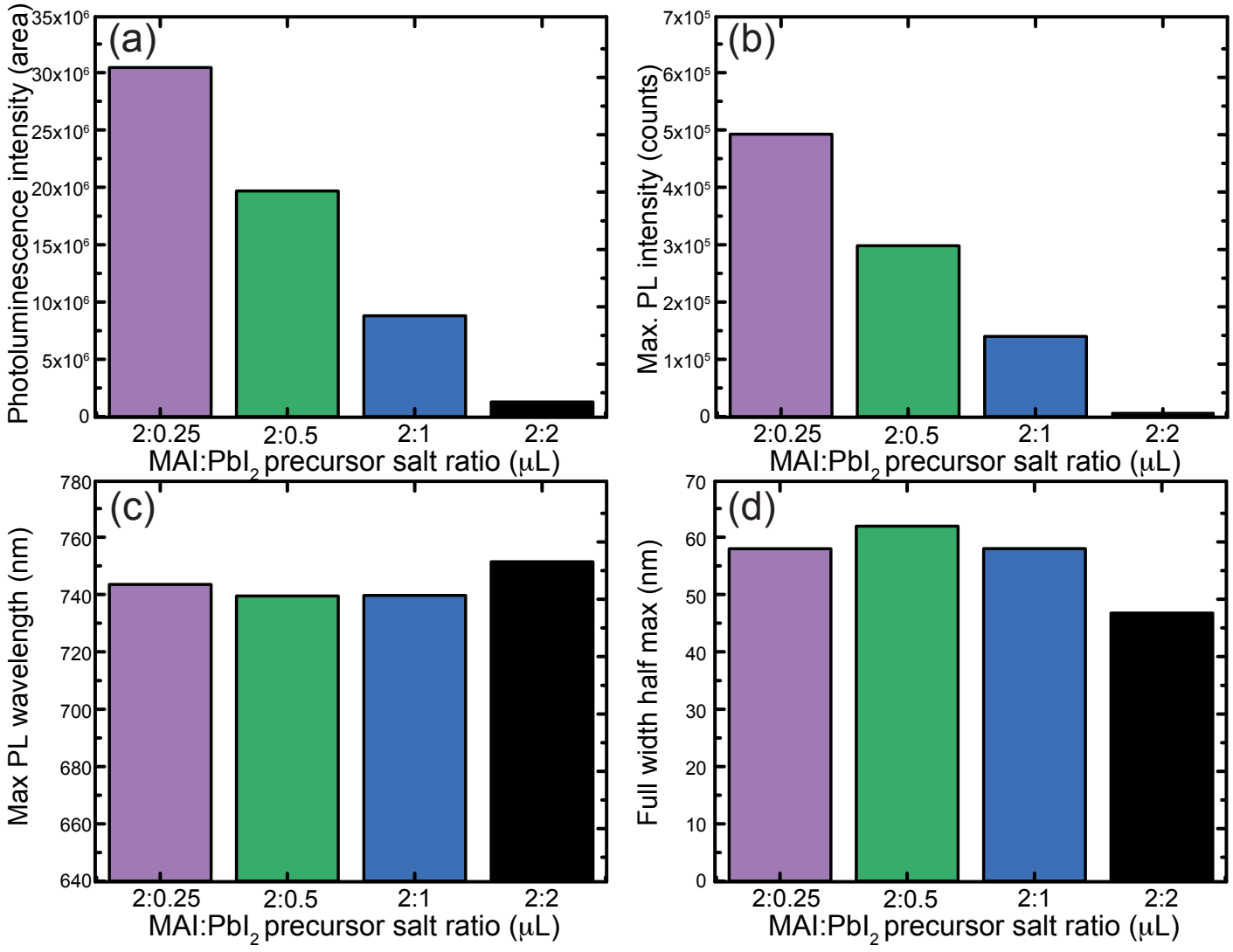

Figure S2 Comparison of the photoluminescence peak properties as a function of the precursor salt ratios (a) integrated area (b) maximum intensity (c) emission wavelength at peak maximum (d) full width half max (FWHM)

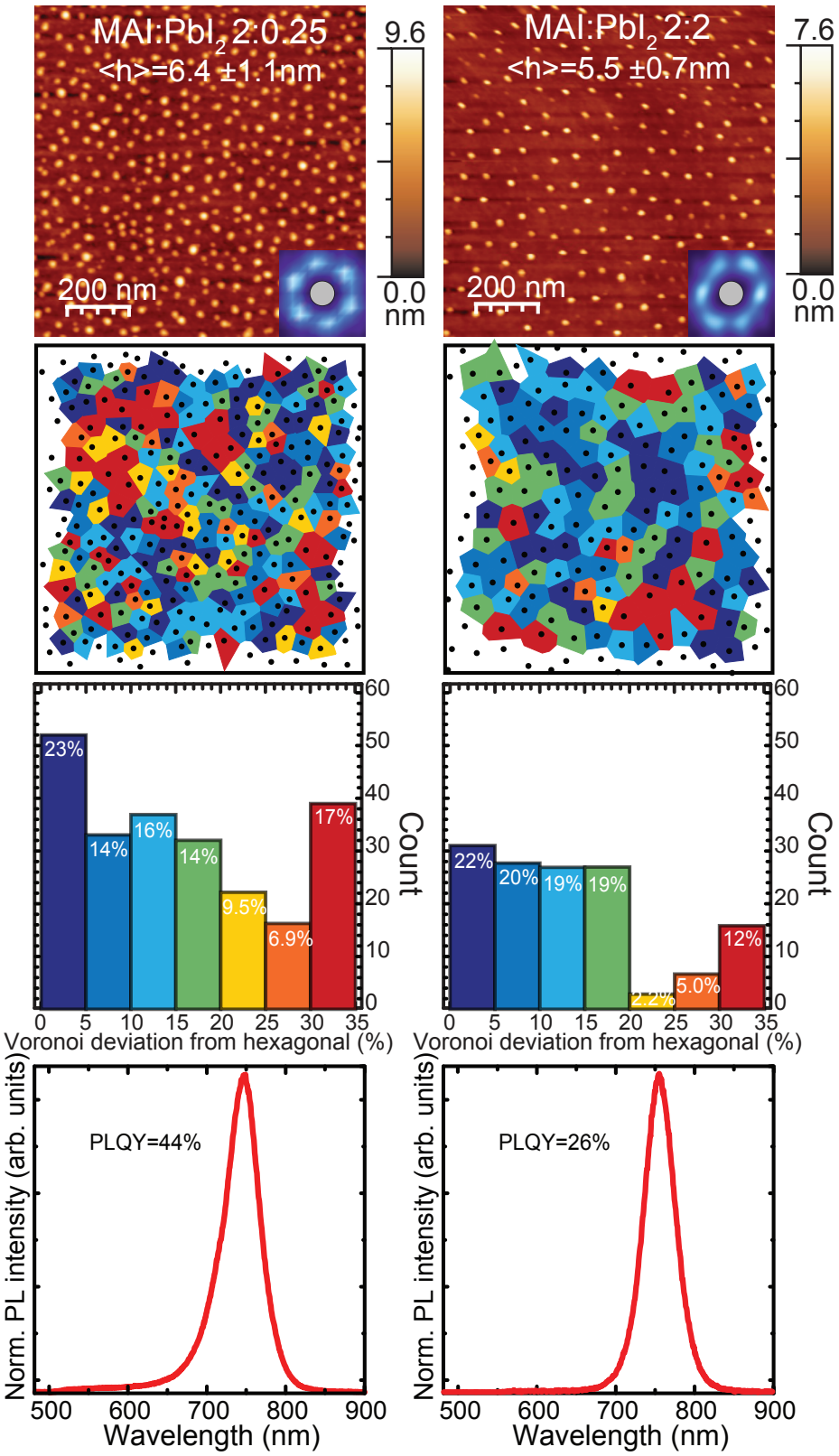

Figure S3 AFM images of $MAPbI_3$ nanoparticles with different precursor salt ratios. The Voronoi tessellations are used to quantify order where the colour indicates the deviation of the cell area relative to a perfect hexagonal lattice, the histogram of the probability distribution of the deviation with respect to the hexagonal cell area is also shown. Normalized photoluminescence spectra with the photoluminescence quantum yield is included in the bottom row.

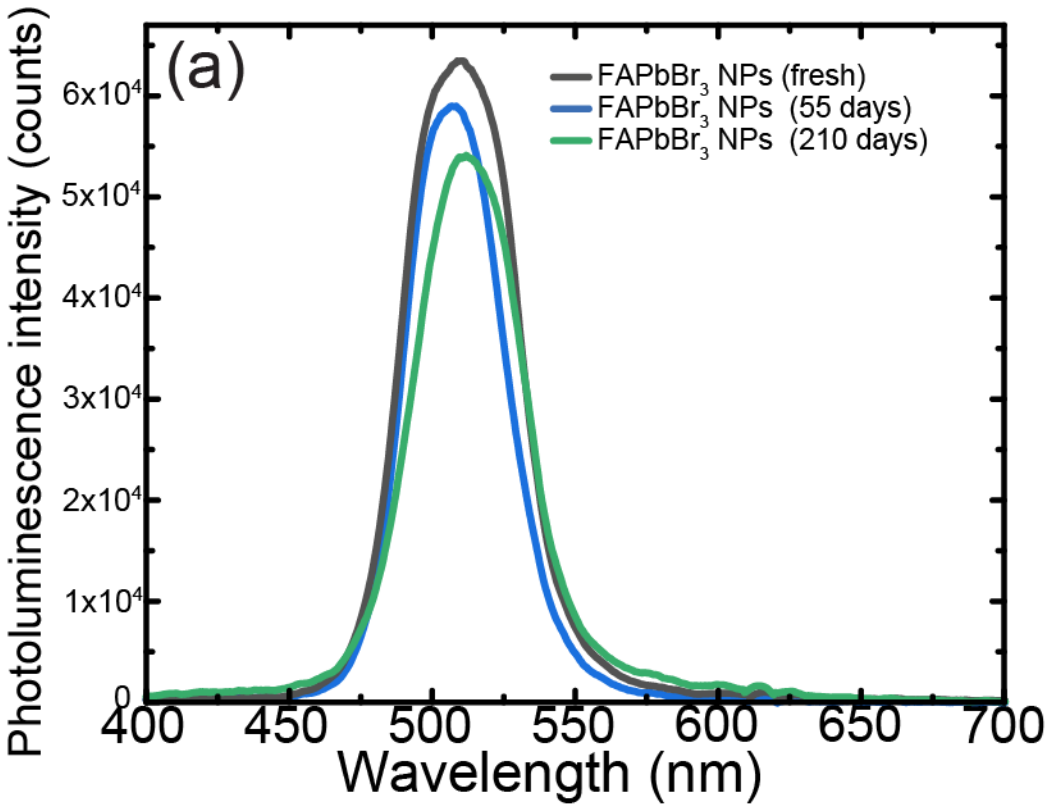

Figure S4 Photoluminescence spectra for micelle encapsulated $FAPbBr_3$ nanoparticles spin coated on Si substrates and exposed to the ambient atmosphere for various lengths of time.

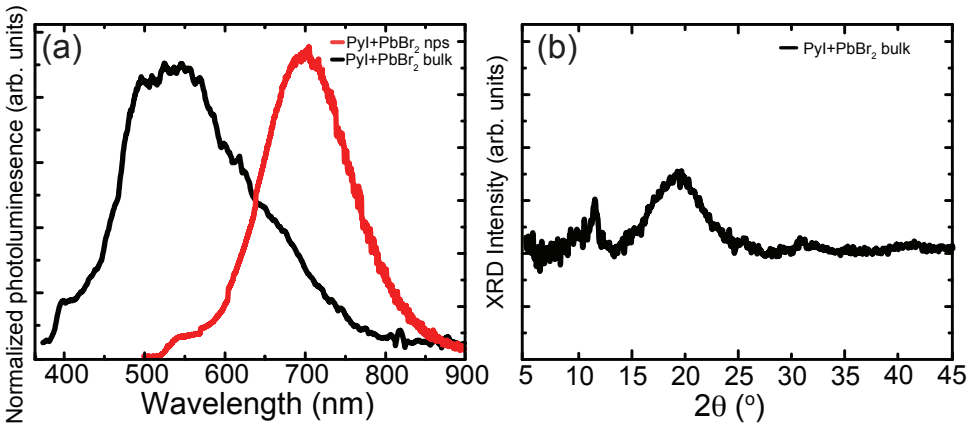

Figure S5 (a) Photoluminescence spectra of drop-cast solutions on Si substrates produced from adding PyI and $PbBr_2$ to o-xylene solutions with and without PS-b-P2VP micelles (b) XRD spectrum of PyI and $PbBr_2$ mixed in o-xylene solutions to produce bulk precipitates.

The powder diffraction simulation function on Vesta was used for the .cif files for each perovskite. For the simulation of $PyPbBr_3$, the iodine atoms were replaced with bromine atoms, inducing slight changes in the crystal structure due to the introduction of the smaller bromine ion, while maintaining the same space group. The calculations were done without periodic boundary conditions. The unit cell parameters and space group for each crystal are given in the table below.

$PyPbI_3$					
a	b	c	alpha	beta	gamma
9.31170	9.31170	8.10800	90.0000	90.0000	120.0000
Unit-cell volume = 608.838770 ^{3}					
Space group name P 63/m m c					
$PyPbBr_3$					
9.31170	9.31170	8.10800	90.0000	90.0000	90.0000
Unit-cell volume = 703.026456 ^{3}					
Space group name P 63/m m c					

Table S1 Resultant crystal structure for simulated $PyPbI_3$ and $PyPbBr_3$ crystals in Vesta.

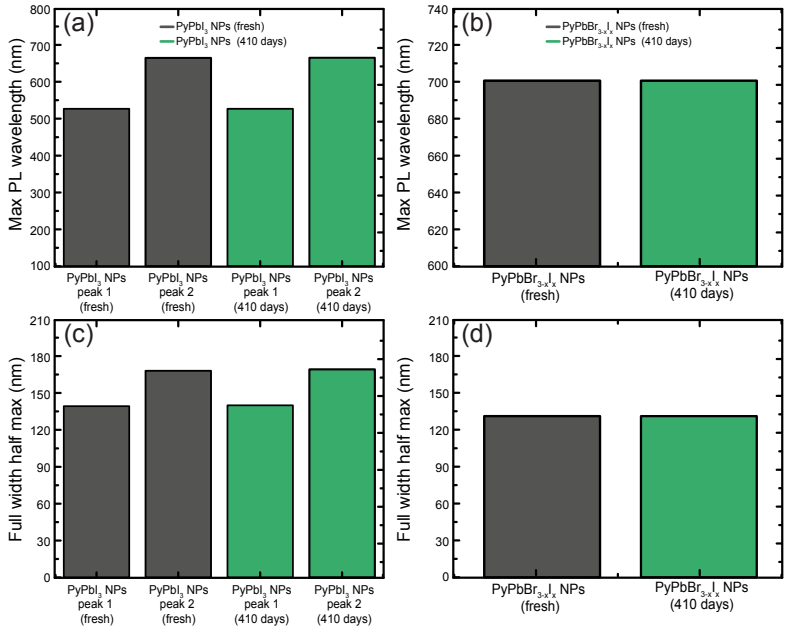

Figure S6 Comparison of the photoluminescence peak properties for Py based perovskite nanoparticles (a-b) emission wavelength at peak maximum (c-d) full width half max (FWHM). Note that the $PyPbI_3$ nanoparticles exhibit a broad emission that can be deconvoluted into two peaks, emission attributed to the hexagonal phase observed in the XRD pattern at around 530nm, as well as a peak at 660 nm that appears to be due to the bulk phase.

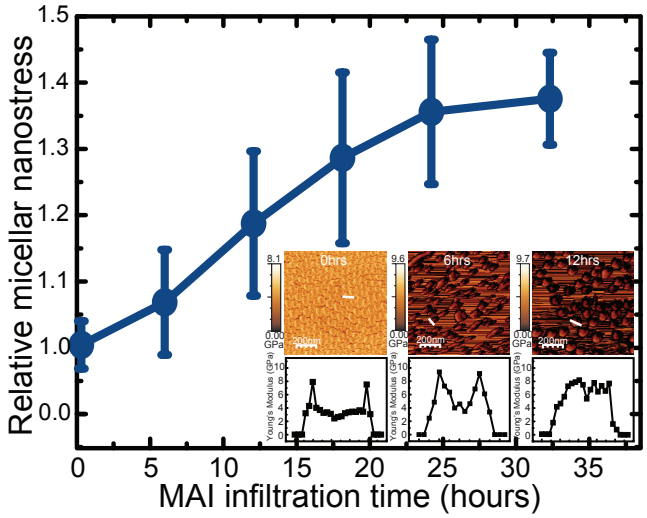

Figure S7 Developed stress inside the micelle during salt loading determined by taking the ratio of the unloaded to loaded micelle

Quantitative nanomechanical property mapping (QNM) AFM was done using a Bruker Bioscope Catalyst with an RTESPA probe. For each round of measurements, the probe was calibrated using a relative method of calibration with a sample of known modulus. The calibration first involved the calculation of the deflection sensitivity by ramping the probe into a clean sapphire substrate. A minimum of three ramps were done and the average deflection sensitivity was used. The probe was then withdrawn from the substrate and a thermal tune was preformed to calculate the spring constant. Lastly, a polystyrene sample of known modulus provided was loaded and imaged. The tip radius was adjusted until the measured modulus agreed with the known modulus. The elastic modulus was determined by taking a line profile through 100 micelles by matching the coordinates in the topography channel to the elastic modulus channel in WSxM. Due to the variability in Young's modulus within a micelle, the elastic modulus for each micelle was determined by taking the average of the centre points of the line profile. The number of points averaged to determine the modulus also varied due to a range in the size of micelles measured. Typically, 10 points were taken for each micelle. The modulus measurements for each micelle were fit using a Gaussian approximation to calculate the average modulus value and error for the unloaded and loaded micelles. The QNM sample preparation is similar to the AFM sample preparation procedures, with the exception for the spin speed being 8000 rpm to promote sparse dispersion.

The inset to Figure S7 shows the Young's modulus maps for precursor loading of micelle at various loading times. They were created by calculating the elastic modulus at each AFM interaction point using the Derjaguin-Müller-Toporov (DMT) model. The DMT model calculates the reduced elastic modulus by fitting the DMT model to the unloading portion of the force-indentation curve (Eq. (1)).[1]

$$F_{tip} = \frac{4}{3}E^* \sqrt{Rd^3} + F_{adh} \tag{1}$$

Where E^* is the reduced elastic modulus, F_{tip} is the force on the AFM tip, F_{adh} is the adhesion force between the AFM tip and the sample (the lowest point on the retract curve), R is the radius of the AFM tip, and d is deformation depth.[1]

The reduced elastic modulus (E^*) can be related to the sample elastic modulus (E_s) by

$$E^* = \frac{(1-\nu_t^2)}{E_t} + \frac{(1-\nu_s^2)}{E_s} \tag{2}$$

In Eq. (2), E_t is the elastic modulus of the AFM tip, ν_t is the Poisson's ratio of the AFM tip, and ν_s is the Poisson's ratio of the sample.[1] As the AFM tip is much stiffer than the sample, we assume E_t to be infinite, causing the first term of the equation to become negligible[1]. The resulting modulus maps produced by the Bruker QNM technique represent the sample elastic modulus (E_s).

The bottom row of the insets to Figure S7 show the line profile through a representative micelle under different loading times. In the empty micelle case at 0 hrs, a dip in the modulus is observed through the centre of the micelle, which can be explained as a result of intrinsic differences between the elastic modulus of the PS and P2VP block, as P2VP forms the core of the micelle and PS the corona[2]. Additionally, this can also result from the the orientation of the co-polymers relative to the tip around the spherical micelle – closer to the edge of the micelle they are expected to be oriented in a lamellar stack, while at the centre, they are standing up-right relative to the AFM tip. It is relatively easier for the AFM tip to penetrate between the up-right PS chains, than to deform the PS backbone. Once the micelle is loaded with precursor salt, the dip through the core relative to the corona of the micelle becomes less pronounced, eventually forming a stiffened core. As the Young's modulus is a material parameter, we can take the local modulus variation results from the stress transfer through the polymer due to the presence of the salt inside the micelle core, similar to that suggested by Liu et al[3] for a thermoplastic polymer subjected to strain during heating; thus, we take the relative ratio of the Young's modulus of the loaded micelle core to the unloaded micelle core as a proxy for the variation as the nano stress in each micelle, assuming that the micelle is in the elastic limit[3].

Figure S7 plots the nanostress developed in the micelle due to MAI precursor infiltration against the loading time. With increasing infiltration time, an increase in the stress is observed, which has previously been correlated with the amount of precursor infiltration into the micelle[2,4]. After around 30 hours of infiltration, a plateau is observed suggesting the maximum infiltration has been achieved.

References

[1] Young, T.J.; Monclus, M.A.; Burnett, T.L.; Broughton, W.R.; Ogin, S.L.; Smith, P.A. The Use of the PeakForce TM Quantitative Nanomechanical Mapping AFM-based Method for High-Resolution Young's Modulus Measurement of Polymers. *Meas. Sci. Technol.* **2011**, *22*, 125703. doi:black10.1088/0957-0233/22/12/125703.

[2] Hanta, G. Nanomechanical Dependence of Micelles on Salt Loading Ratios: A Story of Salt Complexation, Micellar Stability, and Nanoparticle Spatial Distribution. Master of Applied Science, McMaster University, Hamilton, Ontario, 2019.

[3] Liu, H.; Liang, X.; Nakajima, K. Nanoscale Strain–Stress Mapping for a Thermoplastic Elastomer Revealed Using a Combination of in Situ Atomic Force Microscopy Nanomechanics and Delaunay Triangulation. *J. Polym. Sci.* **2022**, *60*, 3134–3140. doi:black10.1002/pol.20220345.

[4] Munir, M.; Tan, J.; Arbi, R.; Oliveira, P.; Leeb, E.; Salinas, Y.; Scharber, M.C.; Sariciftci, N.S.; Turak, A. Enhanced Stokes Shift and Phase Stability by Cosynthesizing Perovskite Nanoparticles (MAPbI3/MAPbBr3) in a Single Solution. *Adv. Photonics Res.* **2022**, *3*, 2100372. doi:black10.1002/adpr.202100372.